http://dx.doi.org/10.1063/1.4719983

Lamb Wave Near Field Enhancements For Surface Breaking Defects In Plates.

A R Clough and R S Edwards
Department of Physics, University of Warwick, United Kingdom

E-mail: a.r.clough@warwick.ac.uk, r.s.edwards@warwick.ac.uk

Abstract. Near field surface wave ultrasonic enhancements have previously been used to detect surface breaking defects in thick samples using Rayleigh waves. Here we present analogous surface wave enhancements for Lamb waves propagating in plates. By tracking frequency intensities in selected regions of time-frequency representations we observe frequency enhancement in the near field, due to constructive interference of the incident wave mode with those reflected and mode converted at the defect. This is explained using two test models; a square based notch and an opening crack, which are used to predict the contribution to the out-of-plane displacement from the reflected and mode converted waves. This method has the potential to provide a reliable method for the near field identification and characterisation of surface breaking defects in plates.

Keywords: Laser Ultrasound, Lamb waves, Enhancement, Defect Characterisation

1. Introduction

Early detection of defects in industrial pipework, such as undersea petrochemical transport or coolant transport in nuclear reactors, is important as small cracks are liable to grow into the material when it is placed under stress and exposed to a corrosive environment. This stress corrosion cracking is highly likely to lead to mechanical failures and can have large economic and ecological impact as a result [1]. Cylindrical pipework (transport of materials) and thin sheet-like structures (storage of material) are commonly used for these applications, and techniques sensitive to the sample surface are a focus of research.

An emerging method of nondestructive testing (NDT) of samples uses ultrasonic surface waves, and a variety of wave modes have been successfully used for defect characterisation [2–5]. Many different ultrasonic generation and detection techniques exist, ranging from conventional contact piezoelectric generated ultrasound, to non contact methods such as electromagnetic acoustic transducers and pulsed laser generation [6–8]. The advantages of a non contact technique, such as the pulsed laser generation and laser interferometric detection used in this work, include the ability to scan a material without loading of the sample surface and removing the requirement for ultrasonic couplant, [9]. Movement of the detection point across the sample surface allows changes in the propagation of the generated surface acoustic waves (SAWs) on interaction with a surface breaking defect to be observed [10].

Recent studies of the interaction of Rayleigh surface waves with surface breaking defects have yielded several interesting effects which have been used to develop new methods of defect identification and characterisation. In the near field, ultrasonic enhancement effects have been observed when the detection point or the generation laser passes over the defect [2, 10–13]. For the enhancement observed as the detector moves over the defect, the enhancements have been shown to be due to a superposition of the incident wave with reflected and mode converted waves produced by interaction with the defect [3, 14–16].

As the sample thickness is reduced, the surface wave becomes a Lamb wave (figure 1) and an understanding of the interaction of these waves with surface breaking defects is needed in order to interpret the near field interactions. Guided waves can be used to probe the structure over long distances [17, 18]. However, long distance examination of a structure only gives information about the far field interactions of the ultrasonic waves with the defect, and useful near field information

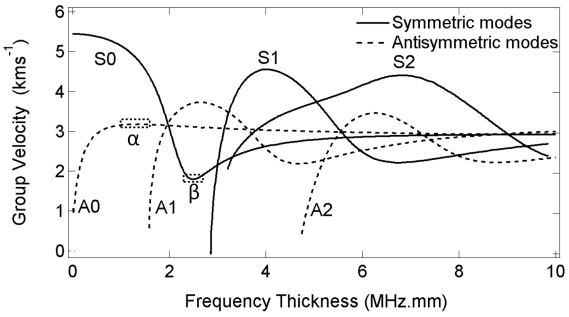

Figure 1: Group velocity dispersion curve for Lamb waves in Aluminium. Frequency range of interest is shown by dashed boxes for the A0 mode (α) and S0 mode (β).

is lost. This near field information can be used to give detailed information on the geometry and severity of the defect, information which is difficult to obtain from far field data due to overlap of signals or attenuation of data.

Previously, near field enhancements have been identified through a simple tracking of the peak to peak amplitude of the Rayleigh wave across the length of a scan [15]. However, the interaction of Lamb waves with surface breaking defects is complicated by the fact that multiple modes exist within a sample, and at any given time there exist at least two modes, the antisymmetric and symmetric fundamental modes [4]. The phase velocity of Lamb waves, C_p, can be solved analytically and converted into the expected group velocity, C_g, which is given as a function of the frequency-thickness product, fd, of the system, [4]

$$c_g = c_p^2 \left[c_p - (fd) \frac{dc_p}{d\,(fd)} \right]^{-1}. \tag{1}$$

The velocity of propagation of these modes depends upon the frequency-thickness product for the sample, and for a broadband generation source there will be multiple modes. The regions shown bounded by dotted lines in figure 1 (α and β) are of interest as the wave displacement here is primarily out-of-plane, and hence standard laser interferometry is particularly sensitive to the modes in this region [4, 25].

In this paper we examine the near field interactions of Lamb waves with surface breaking defects as the detector passes over the defect. Time frequency representations are used to identify the Lamb modes and enable the tracking of

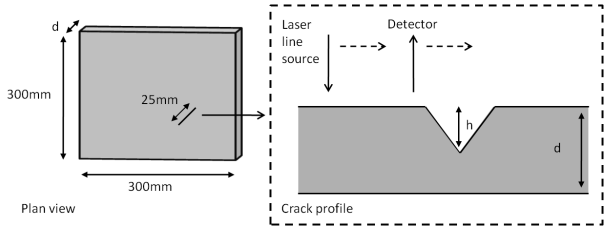

Figure 2: Experimental sample showing scanning schematic and defect geometry.

specific frequency thickness regions of a given wave mode, irrespective of mode overlapping in the time domain. Surface wave enhancements are observed for a range of defect depths in several sheet thicknesses. The observed enhancement is described through the implementation of two test models, for interaction with a square based notch [20] or an open mouthed crack [21].

2. Experimental and Model Details

Investigations were carried out on a range of aluminium samples, of dimensions 300 x 300 x d mm, where d is the sheet thickness (figure 2), for d ranging from 0.5 to 1.5 mm. V-shaped defects of length 25 mm and depth h, from 5 to 100 % of the total sheet thickness, were machined normal to the face of each sheet using a laser micro-machining system, and were positioned so as to reduce backwall reflections at the detector [22]. For defects in the thinnest sheets, $d = 0.5$ mm, localised heating from the machining laser meant that accurate depths could not be assured, and hence defects were produced through conventional milling.

Experiments were performed using a laser generator and a laser detector held at a fixed separation from one another, ensuring that attenuation and dispersion of signals were minimised. Generation used a pulsed Nd:YAG laser (1064 nm wavelength with 10 ns pulse duration) filtered such that it acted as a thermoelastic (non-damaging) source [23], and focused into a line source with dimensions 6 mm by 300 μm. This produces a directional broadband Lamb wave source containing several distinct wave modes which propagate at the velocities and frequencies shown in figure 1 [24].

Detection used an IOS two-wave mixer laser interferometer, which provides out-of-plane displacement data on the sample surface [25]. The IOS detector has a bandwidth of 125 MHz with a laser spot size of 200 μm, and does not require sample

surface preparation. Averaging of 64 data samples was used, and scans were carried out by moving the sample past the generator and detector on an automated linear stage with steps of 50 μm (figure 2).

Simulations were carried out using the Finite Element Method (FEM) software package PZFlex, in which a 3D model was generated [26]. A dipole force on a line of elements was used to simulate the laser generation [27]. The edges of the plate were set to be absorbing to minimise the effect of backwall reflections, and symmetry was used to reduce the size of the model and decrease computational time. The out-of-plane displacements were recorded on a line of nodes in the near field region of the defect.

3. Results

As the detector was scanned across the near field of the defect a set of data was produced containing out-of-plane displacement data as a function of time, with a typical A-scan shown in figure 3(a). Stacking the A-scans together gives a B-scan (figure 3(b)) where the greyscale represents the amplitude of the surface displacement at the detection point, allowing visual tracking of wave modes. We observe an interaction between reflected and mode converted features originating at the defect (positioned at 0 mm) and the incident wave mode; however, this interaction is difficult to quantify due to overlapping modes. Hence we use a time frequency representation. For simplicity and ease of calculation the sonogram time frequency representation was chosen [19]; this windows the time-amplitude data into equal sections, smooths the sections using a Gaussian window, and then performs a fast Fourier transform (FFT).

At each detection point a sonogram was produced, with examples shown in figure 4, where the colour scale gives the magnitude of each frequency component. Using the group velocities calculated from equation 1, with knowledge of the source to detector separation, one can overlay the expected arrival times onto the sonograms and thus identify the various wave modes present. Figure 4(a) shows a sonogram for a scan taken in the far field of the defect, whereas 4(b) is from the near field of the defect where we have interactions between incident and mode converted wave forms. A large increase in magnitude of the A0 mode is seen in some regions, as expected. An increase in the magnitude of the S0 wave is also visible at higher frequencies.

Time frequency representations enable the enhancement of a specific wave mode

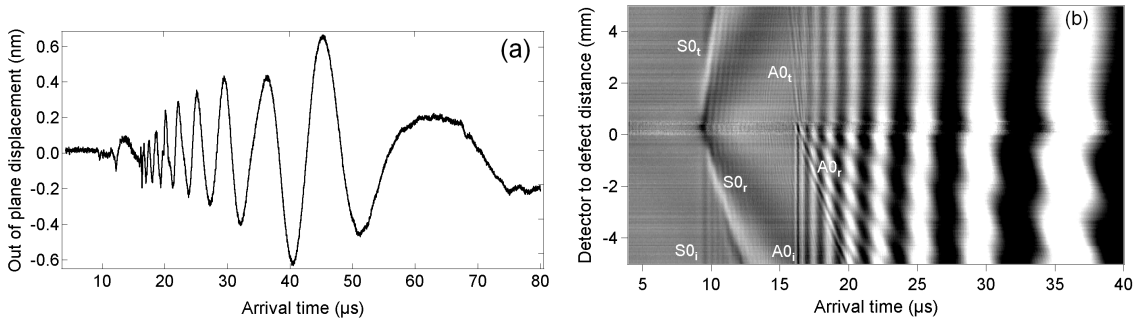

Figure 3: (a) Multimodal Lamb wave A-scan (0.5 mm sheet), (b) B-scan for 0.5 mm sheet with 0.375 mm deep defect. Incident (i), reflected (r) and transmitted (t) fundamental modes are labelled.

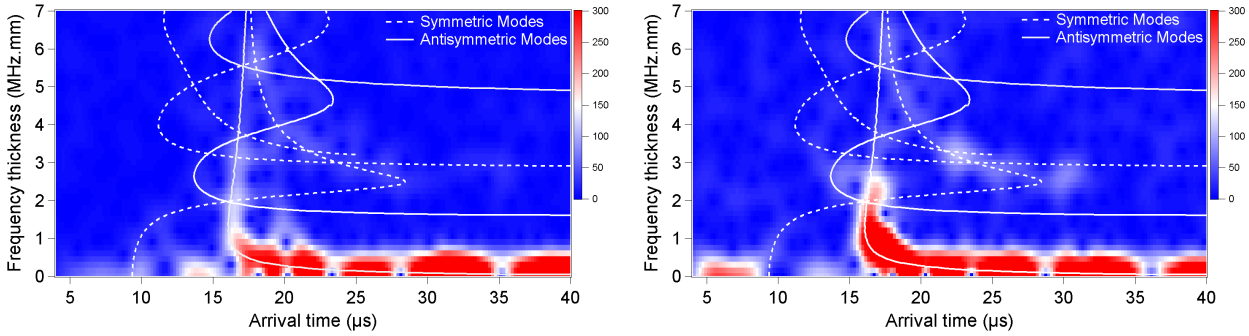

Figure 4: Time frequency representations for 1.5 mm thickness sheet with 100 % through thickness defect for (a) no defect region and (b) enhanced scan position.

to be studied without interference from higher order modes. For each wave mode the total wave displacement is comprised of particle movement in both the in-plane and out-of-plane directions, where the ratio of in-plane to out-of-plane displacement is dependent upon the frequency-thickness product ([4] and section 4). The detector used here is sensitive to the out-of-plane motion at the sample surface, and therefore a focus on the fundamental A0 wave mode is important as, at the plate thicknesses studied, this has a large out-of-plane displacement on the top surface of the plate [4]. For an incident wave mode which is primarily composed of in-plane displacements,

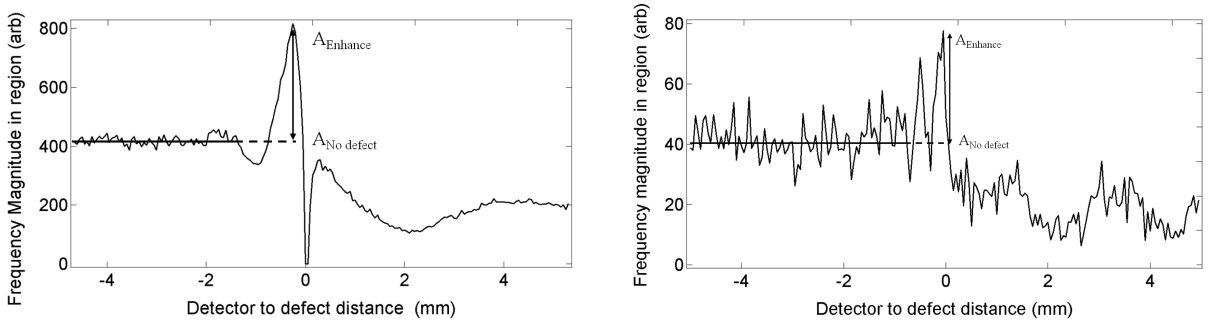

Figure 5: Variation in peak magnitude within chosen region across scan. Enhancements can be observed in many different frequency regions; shown here are the enhancements in the (a) A0 region and the (b) S0 region.

such as the S0 mode between 20 and 30 μs and around 3 MHz.mm, the detection system is not very sensitive. However, if the incident S0 mode should be mode-converted at a defect to a mode with larger out-of-plane displacement, such as the A0 mode, then the observed signal will be larger.

To quantify the enhancement of the signals due to reflection and/or mode conversion, the magnitude in a particular region of the time-frequency plot is measured. Here, the A0 signal was windowed as $1.0 \leq fd \leq 1.6$ MHz.mm and $15.5 \leq t \leq 16.5$ μs (region α in figure 1), with the peak magnitude within this region recorded for the entire scan distance. The magnitude behaviour is shown in figure 5(a), and enhancement factors, E_f, were calculated by taking the ratio of the enhanced magnitude, $A_{Enhance}$, to that which would have been measured if no defect was present, $A_{NoDefect}$;

$$E_f = \frac{A_{Enhance}}{A_{NoDefect}}. \tag{2}$$

To illustrate the versatility of this approach, the peak magnitude of the S0 mode at higher frequency-thickness has also been measured across a scan (figure 5(b)), for magnitude analysis in the region $2.3 \leq fd \leq 2.6$ MHz.mm and $27.9 \leq t \leq 28.7$ μs, corresponding to the S0 wave mode in region β in figure 1. In this frequency-thickness region we expect enhancements due to interactions between the incident and reflected S0 waves, and mode converted A0 and A1 modes following interaction with the defect,

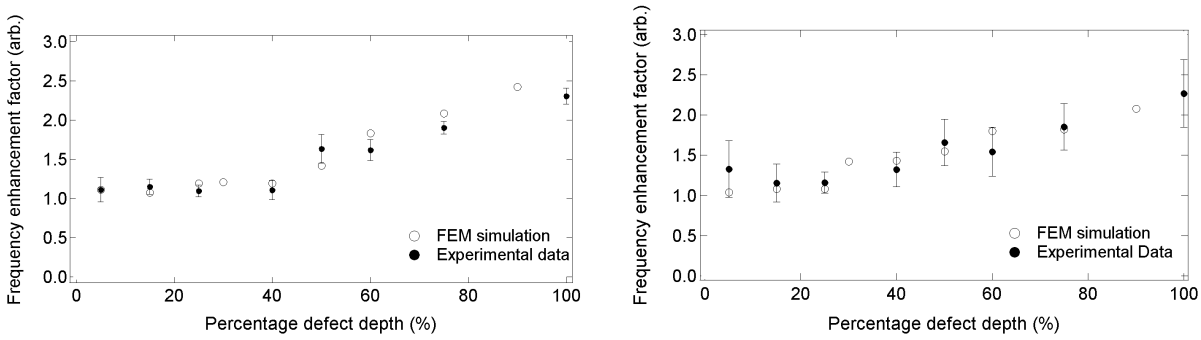

(a) (b)

Figure 6: Enhancement factors in a 1.5 mm sheet for both experimental and FEM simulation as a function of percentage defect depth for both (a) A0 and (b) S0 waves.

with the presence of extra modes giving a different enhancement pattern to that of the A0 mode.

Enhancement factors were calculated for each defect depth in each sheet thickness, for both the experimental and FEM data, and results are shown in figure 6 for the 1.5 mm thick sheet. Similar results were observed for both the 0.5 mm sheet and 1.0 mm sheet and the A0 enhancement can be seen in figure 10. Results show a clear dependence of the enhancement factor on the depth of the defect. Small differences between the experiment and the model arise primarily from the fact that the model output gives the displacement value on a single square node, whereas the experimental displacement is an average across the spot size of the detector (radius $= 200$ μm).

4. Discussion

The relationship between enhancement and defect depth can be explained in terms of superposition of the various possible reflections and mode conversions arising from interaction of the incident A0 mode with the defect. During interaction some fraction of the incident A0 mode will be reflected, while some will be mode converted into a S0 mode [4, 20, 21]. Constructive interfere of the modes will contribute to the total displacement observed by the detector, with an increase in the total out-of-plane displacement showing as an enhancement. In order to quantify this enhancement

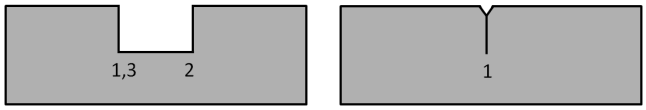

Figure 7: Defect schematic for test models, showing (a) square based notch and (b) open mouthed crack.

the wave modes need to be identified, and the portion of the incident wave energy in the out-of-plane calculated, in order to calculate their contribution to the overall out-of-plane displacement detected by the laser interferometer.

Two different defect models are used to explain the observed variation in enhancement factors with depth, allowing consideration of the reflection and mode conversion for two defect geometries. The first models the defect as a square based notch [20], while the second uses a crack opening just at the surface [21], as shown in figures 7(a) and (b) respectively. Although neither of the test models is a true reflection of the v-shaped defects used in the experiments, there are some similarities, with the open mouth defect being similar to a shallow defect while the square based notch has similarities with a deep defect. Both models consider only the fundamental S0 and A0 wave modes.

The interaction of the A0 mode with the defect is expressed in terms of the reflection and transmission coefficients for each possible reflection and mode conversion. In the case of the square based notch, this involves tracking the possible modes across three interaction interfaces (whenever a thickness change occurs, shown in figure 8), whereas in the case of the open mouthed crack, this interaction only occurs at the single crack interface. These new waves will travel backwards with respect to the incident wave mode and interfere to produce a superposition of wave modes and hence an enhancement.

Table 1 shows the reflection and transmission coefficients for an A0 wave mode incident on a defect with a depth which is 50 % of the through thickness of the plate for both the open mouthed crack interface, and the left and right hand sides of the square based notch, taken from [20, 21]. For a given interaction the reflection, R, and transmission, T, coefficients must follow [20]

$$R^2 + T^2 \leq 1. \tag{3}$$

Table 1: Examples of reflection and transmission coefficients for a 50 % depth defect at $fd = 1.12$ MHz.mm. Values are shown for the open mouthed crack and interfaces 1&2 of the square based notch.

Model type	Open mouth		Square Notch (1)		Square Notch (2)			
Mode conversion	A0 → A0	A0 → S0	A0 → A0	A0 → S0	A0 → A0	A0 → S0	S0 → A0	S0 → A0
Reflection coefficient	0.28	0.14	0.2625	0.155	0.325	0.175	0.3	0.162
Transmission coefficient	0.86	0.14	0.925	0.225	0.925	0.125	0.875	0.225

Considering first the open mouthed crack shown in figure 7(b) with the single interface [21]; one expects the incident A0 mode to be reflected as an A0 mode and mode converted to a reflected S0 mode.

For the square based notch (figure 7(a)) there are three interactions to consider, as shown in figure 8. At each of these interactions one must consider the transmission and reflection coefficients [20]. For example, at the first interface an incident A0 mode produces a backward traveling reflected A0, a backward traveling mode converted S0, and two forward traveling modes; a transmitted A0 and a transmitted mode converted S0 [20]. The two forward traveling modes will continue to the second interface where they will undergo similar reflection and mode conversion. The enhanced signal is then a superposition of the incident A0 mode and all of the reflected and mode converted waves. The arrival times of the backward traveling waves are dictated by the opening size of the notch, and hence a spread in arrival times is expected; this has the effect of spreading the enhancement peak.

Furthermore, Lamb wave modes possess both in-plane and out-of-plane wave motion; the experiments detailed here are sensitive only to the out-of-plane displacements. Therefore, in order to directly compare the test models and the experimental results, one must predict the out-of-plane displacement expected at the enhancement point by identifying the contributions from the individual wave modes. The in-plane and out-of-plane displacements for the allowed A0 and S0 modes at a

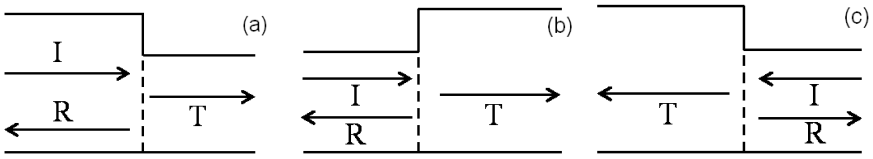

Figure 8: Square based notch scattering interactions at (a) interface 1, (b) interface 2 and (c) interface 3. Arrows show direction of incident (I), reflected (R) and transmitted (T) waves.

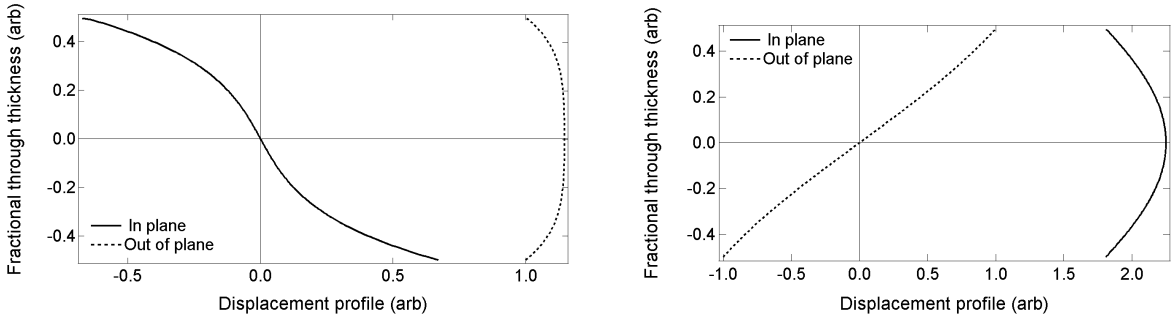

Figure 9: Out-of-plane and in-plane material displacements for (a) A0 wave modes and (b) S0 wave modes in 0.5 mm thick sheets for frequency-thickness of 1.3 MHz.mm

frequency-thickness of 1.3 MHz are shown in figure 9, calculated using the method outlined by Rose [4], as a function of the position through the plate thickness.

Considering an incident A0 amplitude of A_0 at the measured frequency-thickness, the amplitude of each reflected or mode-converted wave mode, A_n, can be calculated using the reflection coefficients (examples given in table 1). Similarly, for each mode the proportion of the wave energy in the out-of-plane displacement, Z_n, can be calculated using the method used to produce figure 9. The maximum possible total out of plane displacement, Z_E, at the enhancement point can then be calculated by considering a direct superposition of all wave modes using

$$Z_E = \sum Z_n.A_n. \tag{4}$$

As an example, for the 50 % defect depth open mouth crack considered in table 1, one would expect relative contributions of 100 % of the incident amplitude of the incident

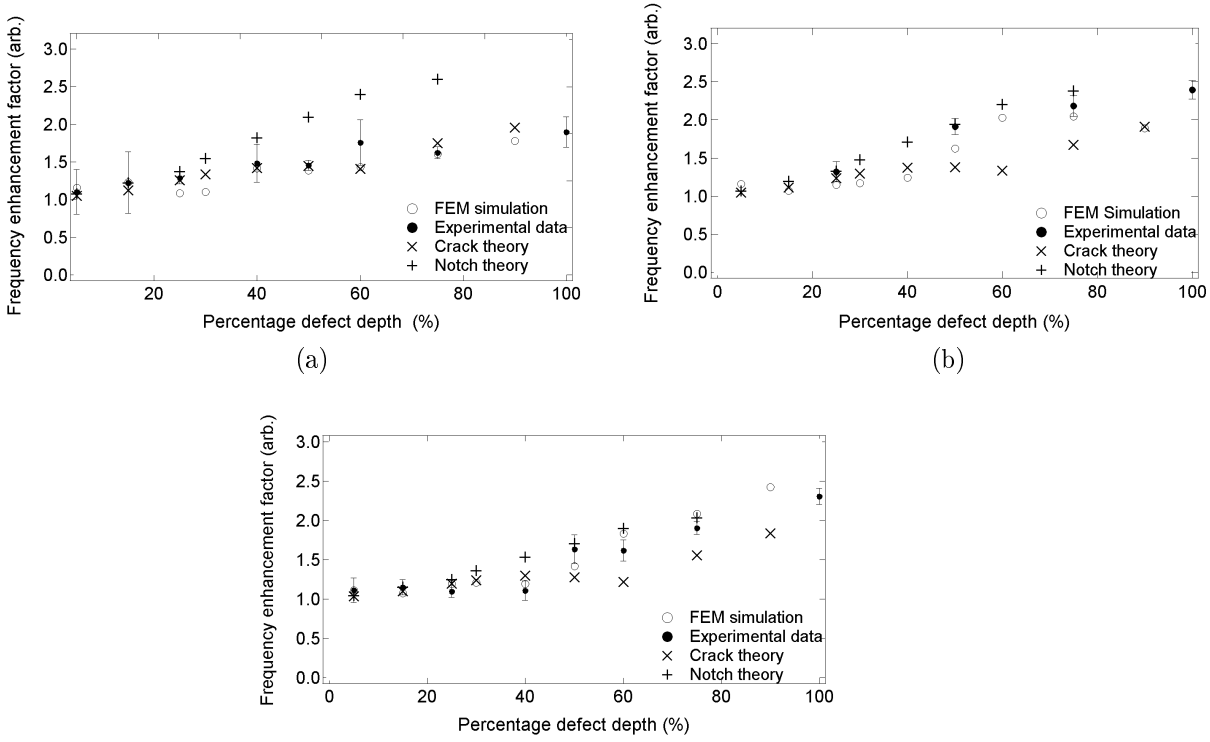

Figure 10: Enhancement factors for experimental, simulation and test model data as a function of defect depth for varying sheet thicknesses; (a) 0.5 mm, (b) 1.0 mm and (c) 1.5 mm.

A0, 28 % of this amplitude from the reflected A0 and 14 % of this amplitude from the mode converted reflected S0 mode at the enhancement point. The enhancement factors can then be calculated as the ratio of the predicted out-of-plane displacement from the superposition at the enhanced point to that expected if only the incident wave mode were present (no defect case).

Measured and calculated enhancement factors are shown in figure 10, and show very good qualitative agreement. This shows that the enhancement can be considered as a superposition of incident, reflected and mode-converted waves, and that the exact enhancements will depend on the exact geometry of the defect. Neither test model takes into account the gradual change in the wave velocity expected

as the frequency-thickness changes for a v-shaped defect, and it has been shown that this will affect the enhancement of Rayleigh waves by increasing the magnitude of the frequency content in the lower frequency-thickness regions of the dispersion curves [28]. This shift towards lower frequency-thickness is not taken into account by either model, which are both based on a sudden change of thickness with a singular change to a new wave mode. However, the good agreement between the calculated and measured enhancement factors shows that the enhancements reported here for a detector passing over a defect can accurately be described by considering reflection and mode-conversion at the defect.

5. Conclusions

Previous work has shown the feasibility of scanning laser detection to characterise surface breaking defects in the near field through the use of surface wave enhancements in Rayleigh waves [10]. We have shown that surface wave enhancement is present in Lamb wave supporting samples at a range of frequency-thicknesses, and that the magnitude of the enhancement is dependent upon the severity of the defect depth. Using time-frequency representations to identify individual wave modes within the sample allows the tracking of the peak magnitude of a given mode in a given frequency-thickness region. This enables the changes in the propagation of the Lamb wave to be monitored across the near field, with enhancement behaviour observed near the defect region.

Comparison between the out-of-plane displacement enhancements observed in experiments and finite element method simulations has shown good agreement and allowed the formation of a model to explain the observed enhancement. Using two test models, a square based notch and an open mouthed crack, the expected wave modes present at the enhancement point have been identified through consideration of the allowed mode reflections and mode conversions arising from interaction with the defect. The distribution of the incident wave energy present in each mode has been calculated through the use of transmission and reflection coefficients for the defect interaction, and has been used to predict the expected contributions to the observed out-of-plane displacements at the enhancement point. Calculated enhancement factors show very good agreement with those obtained from experimental and simulated data. Small differences between the test models and the experimental data are attributed to the difference in defect geometry between the

models and the actual v-shaped defect.

Acknowledgements

This work was funded by the European Research Council under grant 202735, ERC Starting Independent Researcher Grant.

References

[1] The National Physical Laboratory 2000 *"Report on Stress Corrosion Cracking"*

[2] Dixon S, Cann B, Carroll DL, Fan Y and Edwards RS 2008 *Nondestructive Testing and Evaluation* **23(1)** 25-34

[3] Jian X, Dixon S, Guo N and Edwards RS 2007 *J. Appl. Phys.* **101** 064906

[4] Rose JL 1999 *"Ultrasonic Waves in Solid Media."* (Cambridge University Press)

[5] Benz R, Niethammer M, Hurlebaus S and Jacobs L 2003*J. Acoust. Soc. Am.* **114(2)** 677-685

[6] Dewhurst RJ, Edwards CE, McKie ADW and Palmer SB 1987 *Ultrasonics* **25** 315-321

[7] Jian X, Dixon S, Grattan KTV and Edwards RS 2006 *Sensors and Actuators: A. Phys.* **128** 296-304

[8] Hutchins DA, Dewhurst RJ, Palmer SB and Scruby CB 1987 *Appl. Phys. Lett.* **38(9)** 677-679

[9] Scruby CB 1989 *Ultrasonics* **27** 195-209

[10] Edwards RS, Dixon S and Jian X 2004 *J. Phys. D: Appl. Phys.* **37** 2291-2297

[11] Edwards RS, Jian X, Fan Y and Dixon S 2005 *Appl. Phys. Lett.* **87** 194104

[12] Kromine AK, Fomitchov PA, Krishnaswamy S and Achenbach JD 2000 *Materials Evaluation* **58(2)** 173- 77

[13] Arias I and Achenbach JD 2004 *Wave Motion* **39(1)** 61-75

[14] Jian X, Dixon S, Guo N, Edwards RS and Potter M 2006 *Ultrasonics* **44** e1131-e1134

[15] Dutton B, Clough AR and Edwards RS 2011 *NDT&E International* **44** 353-360

[16] Dutton B, Clough AR and Edwards RS 2011 *J. Nondestruct. Eval.* **30(2)** 64-70

[17] Lowe MJS, Cawley P, Kao J-Y and Diligent O 2002 *J. Acoust. Soc. Am.* **112(6)** 2612-2622

[18] Lowe MJS and Diligent O 2002 *J. Acoust. Soc. Am.* **111(1)** 2589-2601

[19] Niethammer M, Jacobs L, Qu J and Jarzynski J 2001 *J. Acoust. Soc. Am.* **109(5)** 1841-1847

[20] Kim B and Roh Y 2011 *Ultrasonics* **51** 734-744

[21] Castaings M, Le Clezio E and Hosten B 2002 *J. Acoust. Soc. Am.* **112(6)** 2567-2582

[22] Burrows SE, Dutton B and Dixon S 2012 . *"Laser generation of lamb waves for defect detection: experimental methods and finite element modelling."* *IEEE Trans. Ultrason. Ferro. Freq.*, in press.

[23] Scruby CB and Drain LE 1990 *"Laser ultrasonics: techniques and applications"* (Adam Hilger, Bristol)

[24] Aindow AM, Dewhurst RJ and Palmer SB 1982 *Optics Communications* **42(2)** 116-120

[25] Klein MB, Bacher GD, Grunnet-Jepson A, Wright D and Moerner WE 1999 *Optics Communications* **162** 79-84

[26] PZFlex version 2.3 developed by Weidlinger Associates Inc., http://www.pzflex.com

[27] Arias I and Achenbach JD 2003 *Int. J. Solids Struct.* **40(25)** 6917-6935

[28] Edwards RS, Dutton B, Clough AR and Rosli MH 2011 *Appl. Phys. Lett.* **99** 094104